Lawrence Berkeley National Laboratory
LBL Publications

Title
FREQUENCY AND WAVE-VECTOR-DEPENDENT DIELECTRIC FUNCTION FOR SILICON

Permalink
https://escholarship.org/uc/item/7x9254w5

Author
Walter, John P.

Publication Date
1971-12-01

eScholarship.org Powered by the California Digital Library
University of California

Submitted to Physical Review

LBL-487
Preprint
c.2

FREQUENCY AND WAVE-VECTOR-DEPENDENT DIELECTRIC FUNCTION FOR SILICON

John P. Walter and Marvin L. Cohen

RECEIVED
LAWRENCE
RADIATION LABORATORY
FEB 11 1972
LIBRARY AND
DOCUMENTS SECTION

December, 1971

AEC Contract No. W-7405-eng-48

TWO-WEEK LOAN COPY

This is a Library Circulating Copy which may be borrowed for two weeks. For a personal retention copy, call Tech. Info. Division, Ext. 5545

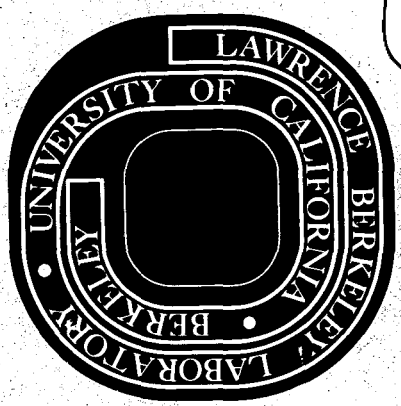

LBL-487
c.2

34

DISCLAIMER

This document was prepared as an account of work sponsored by the United States Government. While this document is believed to contain correct information, neither the United States Government nor any agency thereof, nor the Regents of the University of California, nor any of their employees, makes any warranty, express or implied, or assumes any legal responsibility for the accuracy, completeness, or usefulness of any information, apparatus, product, or process disclosed, or represents that its use would not infringe privately owned rights. Reference herein to any specific commercial product, process, or service by its trade name, trademark, manufacturer, or otherwise, does not necessarily constitute or imply its endorsement, recommendation, or favoring by the United States Government or any agency thereof, or the Regents of the University of California. The views and opinions of authors expressed herein do not necessarily state or reflect those of the United States Government or any agency thereof or the Regents of the University of California.

Frequency and Wave-Vector-Dependent Dielectric Function for Silicon*

by

John P. Walter† and Marvin L. Cohen

Department of Physics, University of California

and

Inorganic Materials Research Division, Lawrence Radiation Laboratory

Berkeley, California 94720

Abstract

The frequency and wave-vector-dependent complex dielectric function $\epsilon(\vec{q},\omega)$ is calculated for silicon. The energy eigenvalues and eigenvectors which are used have been obtained from energy-band calculations based on the empirical pseudopotential method. Explicit results are given in the [100] direction in the range $0 \leq q \leq (2\pi/a)$ and $0 \leq \hbar\omega \leq 24$ eV. A comparison is made between the present results and the results of a calculation of $\epsilon(q,\omega)$ for a free electron gas in the random phase approximation.

I. Introduction

We have calculated the frequency and wave-vector-dependent dielectric function $\epsilon(\vec{q},\omega)$ in the [100] direction for silicon. This is the first calculation of $\epsilon(\vec{q},\omega)$ for a semiconductor in which realistic energy eigenvalues and eigenvectors are used. Previous calculations of dielectric functions have concentrated either on the wave-vector-dependent dielectric function[1] for zero frequency $\epsilon(\vec{q},\omega = 0)$ or on the frequency-dependent dielectric function[2] $\epsilon(\vec{q} = 0,\omega)$. The former case is important in determining the static screening of electric fields, and the latter case is important in analyzing the optical properties of semiconductors because q is approximately zero for optical wave-vectors. The more general dielectric function $\epsilon(\vec{q},\omega)$ describes the screening of a longitudinal field which varies in both space and time. A knowledge of $\epsilon(\vec{q},\omega)$ permits us to obtain the following properties of the solid: the response to weak external longitudinal fields; the density-fluctuation excitation spectrum (energy-loss of a fast charged particle); and the time-dependent correlations between the density fluctuations (plasmon modes).

In the present calculation the real part of the dielectric function $\epsilon_1(\vec{q},\omega)$ is calculated directly, and the imaginary part $\epsilon_2(\vec{q},\omega)$ is calculated using the Kramers-Krönig transformation. The functions $\epsilon_1(\vec{q},\omega)$ and $\epsilon_2(\vec{q},\omega)$ are then used to calculate the imaginary part of the inverse dielectric function $\mathrm{Im}\,\epsilon^{-1}(\vec{q},\omega)$, which is proportional for small q to the energy-loss function of a fast charged particle passing through the solid.

The details of the calculation are given in Sec. II along with the results for silicon. In Sec. III the silicon calculations are compared with a calculation of $\epsilon_1(q,\omega)$, $\epsilon_2(q,\omega)$ and $\mathrm{Im}\,\epsilon^{-1}(q,\omega)$ for a free electron gas in the random phase approximation, that is, the Lindhard[3] dielectric function. A comparison of the various dielectric functions for silicon and the free electron gas illustrates the principal difference between the two cases.

II. Calculations

First we calculate the longitudinal wave-vector-dependent and frequency-dependent dielectric function $\epsilon(q,\omega)$ for silicon which describes the response of a crystal to an electric field parallel to $\vec{q}$ and varying sinusoidally in time:

$$\vec{D}\, e^{i(\vec{q}\cdot\vec{r} - \omega t)} = \epsilon(\vec{q},\omega)\,\vec{E}\, e^{i(\vec{q}\cdot\vec{r} - \omega t)} . \tag{2.1}$$

Using the expression for $\epsilon_1(\vec{q},\omega)$ given by Ehrenreich and Cohen[4], we obtain

$$\epsilon_1(\vec{q},\omega) = 1 + \frac{4\pi e^2}{\Omega q^2} \sum_{\vec{k},c,v} \left|\langle \vec{k},c \left| \vec{k}+\vec{q},v \right\rangle\right|^2 \times \{[E_c(\vec{k}) - E_v(\vec{k}+\vec{q}) - \hbar\omega]^{-1} + [E_c(\vec{k}) - E_v(\vec{k}+\vec{q}) + \hbar\omega]^{-1}\} , \tag{2.2}$$

where $\vec{k}$ is summed over the first Brillouin zone, v labels the valence bands, and c labels the conduction bands. For the purposes of calculation Eq. (2.2) is written as follows

$$\epsilon_1(\vec{q},\omega) = 1 + \frac{4\pi e^2}{q^2}\frac{2}{(2\pi)^3}\sum_{\Delta k,c,v} |\langle \vec{k},c|\vec{k}+\vec{q},v\rangle|^2(\Delta k)^3 \times \{[E_c(\vec{k}) - E_v(\vec{k}+\vec{q}) - \hbar\omega]^{-1} + [E_c(\vec{k}) - E_v(\vec{k}+\vec{q}) + \hbar\omega]^{-1}\}, \quad (2.3)$$

where the summation is over cubes of volume $(\Delta k)^3$ in the first Brillouin zone, with suitable truncations at the zone boundaries. The summation index v spans the top four valence bands and the index c spans the bottom eleven conduction bands. $E_n(\vec{k})$ is the energy eigenvalue of band n at state $\vec{k}$ and $|\vec{k},n\rangle$ is the corresponding eigenvector.

The energy eigenvalues and eigenvectors are calculated using the empirical pseudopotential method, as described in Ref. 2. Since spin-orbit effects are small for silicon, they have not been included in this calculation. The pseudopotential form factors have been adjusted so that the reflectivity and the principal optical gaps agree with experimental measurements.[5,6] Fifteen energy eigenvalues and eigenvectors are computed for each of 3360 points in the Brillouin zone. The coordinates of the grid of calculated points are given by $\frac{1}{16}(2s+1, 2m+1, 2n+1)$ in units of $2\pi/a$, where s, m, and n are integers.

For an arbitrary direction of $\vec{q}$, the summation in Eq. (2.3) must be performed over the entire Brillouin zone. Fortunately, symmetry properties can be exploited to reduce the computation time by a factor of 8 in the [100] direction. The computation time for a particular value of $\vec{q}$ can be reduced by an additional factor of 15 if $\vec{q}$ is chosen such that $(\vec{k}+\vec{q})$ also lies on the grid of calculated points.

For certain values of c, v, $\vec{k}$, $\vec{q}$ and ω, $[E_c(\vec{k}) - E_v(\vec{k}+\vec{q}) - \hbar\omega]^{-1}$ can have singularities and it varies rapidly as $\vec{k}$ varies over the cube of volume $(\Delta k)^3$. For such cases, the cube is divided into 216 equal sub-cubes. The contributions of $(E_c - E_v - \hbar\omega)^{-1}$ are calculated by interpolation and are added together and multiplied by the new volume of $(\Delta k)^3/216$. The values of $|\langle \vec{k}, c | \vec{k}+\vec{q}, v\rangle|^2$ and $[E_c(\vec{k}) - E_v(\vec{k}) + \hbar\omega]^{-1}$ which is not singular very much more slowly and are given the values they assume at the center of the larger cubes.

After we calculate $\epsilon_1(\vec{q},\omega)$, the imaginary part of the dielectric function $\epsilon_2(\vec{q},\omega)$ is calculated by a Kramers-Krönig transform of $\epsilon_1(\vec{q},\omega)$. The imaginary part of the inverse dielectric function Im $\epsilon^{-1}(\vec{q},\omega)$ is then easily computed. Figs. 2-6 display plots of $\epsilon_1(\vec{q},\omega)$, $\epsilon_2(\vec{q},\omega)$ and Im $\epsilon^{-1}(\vec{q},\omega)$ as a function of ω for q = 0, 1/4, 1/2, 3/4, and 1 in units of $2\pi/a$ in the [100] direction. In Ref. 1 we have shown that $\epsilon_1(\vec{q},\omega=0)$ is nearly isotropic with only minor deviations for $\vec{q}$ parallel to the [1, 1, 1] direction. Therefore, we expect that $\epsilon(\vec{q},\omega)$ does not change significantly in shape for other directions of $\vec{q}$.

An indication of the accuracy of the present calculation of $\epsilon_1(q=0,\omega)$ is given by a comparison with a much more accurate calculation done in conjunction with the work on silicon presented in Ref. 6. In this previous calculation 356 points in 1/48 of the Brillouin zone were accurately computed and then the energy eigenvalues and the dipole matrix elements were both determined on a much finer grid of 175,000 points in 1/48 of the Brillouin

zone by means of an interpolation scheme. The comparison in Fig. 1 shows that the present calculation of $\epsilon_1(\vec{q}=0,\omega)$ is approximately correct, and this, in turn, indicates the accuracy of our calculations of $\epsilon(\vec{q},\omega)$.

The numerical accuracy of the Kramers-Krönig transform is excellent; however, the reader should notice that $\epsilon_2(\vec{q},\omega)$ is negative for q = 0, 1/4, for small ω whereas it should be zero because of the energy gap. This incorrect result is caused by small errors in the calculation of $\epsilon_1(\vec{q},\omega)$. Small errors in ϵ_1 and ϵ_2 can cause larger errors in $\mathrm{Im}\epsilon^{-1}$, and for this reason the smaller structure in the plots of $\mathrm{Im}\epsilon^{-1}$ is not to be regarded as accurate.

III. Discussion

In this section we compare the results for the silicon $\epsilon_1(\vec{q},\omega)$, $\epsilon_2(\vec{q},\omega)$ and the $\mathrm{Im}\,[\epsilon^{-1}(\vec{q},\omega)]$ with these functions calculated for a free electron gas in the random phase approximation. This RPA or Lindhard dielectric function has the form

$$\epsilon_1(\beta,\delta) = 1 + \frac{K_S^2}{8\beta q^2}\left\{\left[1-(\beta+\gamma)^2\right]\log\left|\frac{1+\beta+\gamma}{1-\beta-\gamma}\right| + \left[1-(\beta-\gamma)^2\right]\log\left|\frac{1+\beta-\gamma}{1-\beta+\gamma}\right| + 4\beta\right\} \tag{3.1}$$

and

$$\epsilon_2(\beta,\delta) = \frac{\pi K_S^2}{8\beta q^2} \times \begin{cases} \delta, \text{ when } \beta < 1 \text{ and } \delta < |4\beta^2 - 4\beta| \\ 1-(\beta-\gamma)^2, \text{ when } |4\beta^2 - 4\beta| < \delta < |4\beta^2 + 4\beta| \\ 0, \text{ when } \delta > |4\beta^2 + 4\beta| \\ 0, \text{ when } \beta > 1 \text{ and } \delta < |4\beta^2 - 4\beta| \end{cases} \tag{3.2}$$

where $\beta = q/2k_F$, $\delta = \hbar\omega/E_F$, $\gamma = \delta/4\beta$, K_S is the inverse Fermi-Thomas screening length, k_F is the free electron Fermi wavevector, and E_F is the Fermi energy.

$\epsilon_1(\vec{q},\omega)$ for silicon is displayed in a perspective plot (Fig. 7) which more clearly illustrates how ϵ_1 varies in the $(\vec{q},\omega)$ plane. In Fig. 8 we give a similar plot of the Lindhard $\epsilon_1(q,\omega)$ obtained from evaluating Eq. (3.1) for a density of free electrons that give a plasma frequency ω_p identical to the calculated silicon value. (The plasma frequency ω_p is given by the high-frequency zero of $\epsilon_1(\vec{q},\omega)$).

For $q = 0$ and ω small, the silicon ϵ_1 and the Lindhard ϵ_1 differ markedly. In particular, the Lindhard ϵ_1 assumes the familiar form $\epsilon_1(q = 0,\omega) = 1 - \omega_p^2/\omega^2$, which has a singularity at $\omega = 0$. This is in complete contrast with the silicon ϵ_1, which is an increasing positive function for small ω. The significant difference between the two functions at $q = 0$ is that the lower zero of the silicon ϵ_1 occurs at about 4.5 eV, whereas the zero of the Lindhard ϵ_1 occurs at zero. The behavior of the lower zero in ϵ_1 is discussed later in greater detail. For small ω at all non-zero values of q, the silicon ϵ_1 increases with ω until the function reaches a maximum, but for the Lindhard case, ϵ_1 decreases with increasing ω, so that the maximum value of the Lindhard ϵ_1 always occurs at $\omega = 0$.

At high ω for all q the silicon and Lindhard ϵ_1 functions are similar. This is reasonable since at high ω (such that $\hbar\omega$ is much larger than the energy gap), we expect silicon to resemble a free electron gas because the high-energy excited states correspond to loosely bound electrons.

In Figs. 9 and 10 $\epsilon_2(q,\omega)$ is plotted for the silicon and Lindhard cases. Because of the gap, the silicon ϵ_2 is identically zero at small ω while in the Lindhard case ϵ_2 differs from zero for small ω for all q. The Lindhard $\epsilon_2(\omega)$ first increases linearly and then falls quadratically with ω for each q (see Eq. (3.2)). The quadratic dependence is not clearly visible in Fig. 10 because of the perspective nature of the graph and the rapid dependence of ϵ_2 on ω in these regions. As in the case of $\epsilon_1(q,\omega)$, the differences in $\epsilon_2(q,\omega)$ between the silicon and Lindhard cases are most prominent at low q and ω.

Figs. 11 and 12 show $\mathrm{Im}[\epsilon^{-1}(\vec{q},\omega)]$ for the silicon and Lindhard cases. These cases differ considerably. In the Lindhard case the function approaches zero as q and ω approach zero except for the characteristic δ-function at $\omega = \omega_p$. It becomes finite and increases in magnitude as q and ω become larger. The sum rules are satisfied by appropriate contributions at $\omega_p(q)$. The function becomes finite for each non-zero q as ω increases from zero, whereas for silicon the gap in the ϵ_2 spectrum causes the $\mathrm{Im}[\epsilon^{-1}(q,\omega)]$ function to be zero at small ω. Comparison with experiment can be made with optical work[7] and electron energy loss measurements.[8] The agreement is good with respect to amplitude, width and position of the peak, but we caution the reader against taking the small structure near ω_p seriously in Fig. 11. In this energy range ϵ_1 and ϵ_2 are close to zero and small errors are magnified in the $\mathrm{Im}[\epsilon^{-1}(\vec{q},\omega)]$ function.

For the Lindhard case (Fig. 12) pair excitation (lower ω) contributions

to $\mathrm{Im}[\epsilon^{-1}]$ eventually merges with the plasmon contribution at larger q. This occurs for q's where the $\omega(q)$ line satisfying $\epsilon_1[q,\omega(q)] = 0$ enters the continuum. For the present case this happens when $1.176 < qa/2\pi < 1.177$. The upper end of the spectrum is still sharply peaked resembling a plasmon-like contribution. For silicon (Fig. 11) this occurs even at $q = 0$ and the ϵ_2 coming from pair excitations damps the plasmon peak.

It is interesting to examine the q and ω dependence of the zeros of the $\epsilon_1(q,\omega)$ function in the (q,ω) plane. The results are given in Fig. 13. For the Lindhard case the lower zero ω_0 of ϵ_1 occurs at frequencies which are linear in q. This can be seen by expanding the Lindhard function given in Eq. (3.1) for small q and ω. An easier method is to use the precursor to Eq. (3.1):

$$\epsilon(\vec{q},\omega) = 1 + \frac{4\pi e^2}{q^2} \sum_{\vec{k}} \frac{f(\vec{k}+\vec{q}) - f(\vec{k})}{E(\vec{k}+\vec{q}) - E(\vec{k}) - \hbar\omega} \quad . \tag{3.3}$$

For small q, the difference in the Fermi factors becomes

$$f(\vec{k}+\vec{q}) - f(\vec{k}) \approx \vec{q} \cdot \frac{\partial f}{\partial \vec{k}} \approx q\mu\,\delta(k - k_F) \quad , \tag{3.4}$$

where

$$\mu = \frac{\vec{k}\cdot\vec{q}}{kq} \quad .$$

Dropping terms in q^2 in the integrand, the dielectric function becomes

$$\epsilon(q,\omega) = 1 + \frac{K_s^2}{2q^2} \int_{-1}^{1} \frac{\mu d\mu}{\mu - \gamma} = 1 + \frac{K_s^2}{2q^2} \left(2 - \gamma \log \left| \frac{1+\gamma}{1-\gamma} \right| \right) , \quad (3.5)$$

where $\gamma = \omega/qv_F$. The lower zero (which looks like a damped transverse-like mode in the continuum) arises when

$$2 \approx \gamma \log \left| \frac{1+\gamma}{1-\gamma} \right| . \quad (3.6)$$

This condition requires a fairly linear $\omega(q)$ curve, i.e.

$$\omega \approx \frac{5}{6} v_F q \quad (3.7)$$

which agrees well with the computer calculations.

For silicon the lower zero does not result from a linear dispersion curve, but a gap appears in the spectrum. This is the most significant difference between the two dielectric functions. At higher q, the two curves tend to merge, but it is more difficult to calculate the zeros of ϵ_1 in this region of the plane. In other words it is the gap in the spectrum at smaller q which distinguishes the silicon case from the free electron gas case as expected.

References

* Supported in part by National Science Foundation grant GP 13632.

† Present address: Department of Physics, Brandeis University, Waltham, Massachusetts 02154.

1. J. P. Walter and M. L. Cohen, Phys. Rev. B2, 1821 (1970).
2. M. L. Cohen and V. Heine, Solid State Physics 24, 37 (1970).
3. J. Lindhard, Kgl. Danske Videnskab, Mat.-Fys. Medd. 28, 8 (1954).
4. H. Ehrenreich and M. H. Cohen, Phys. Rev. 115, 786 (1959).
5. D. Brust, M. L. Cohen and J. C. Phillips, Phys. Rev. Letters 9, 389 (1962).
6. R. R. L. Zucca, J. P. Walter, Y. R. Shen and M. L. Cohen, Solid State Commun. 8, 627 (1970).
7. H. R. Philipp and H. Ehrenreich, Phys. Rev. 129, 1550 (1963).
8. H. Dimigen, Z. Physik 165, 53 (1961).

Figure Captions

1. Comparison of two silicon calculations $\epsilon_1(q=0,\omega)$. The 70-point calculation is performed as described in this paper and is the less accurate of the two. The 356-point calculation uses five times as many grid points and a much finer interpolated grid of 175,000 points on which to perform the integration.
2. Plots of ϵ_1, ϵ_2 and Im ϵ^{-1} for silicon as a function of $\hbar\omega$ for $\vec{q} = (0,0,0)$.
3. Plots of ϵ_1, ϵ_2 and Im ϵ^{-1} for silicon as a function of $\hbar\omega$ for $\vec{q} = (1/4,0,0)2\pi/a$.
4. Plots of ϵ_1, ϵ_2 and Im ϵ^{-1} for silicon as a function of $\hbar\omega$ for $\vec{q} = (1/2,0,0)2\pi/a$.
5. Plots of ϵ_1, ϵ_2 and Im ϵ^{-1} for silicon as a function of $\hbar\omega$ for $\vec{q} = (3/4,0,0)2\pi/a$.
6. Plots of ϵ_1, ϵ_1 and Im ϵ^{-1} for silicon as a function of $\hbar\omega$ for $\vec{q} = (1,0,0)2\pi/a$.
7. Perspective plot of $\epsilon_1(\vec{q},\omega)$ for silicon
8. Perspective plot of $\epsilon_1(\vec{q},\omega)$ for a free electron gas.
9. Perspective plot for $\epsilon_2(\vec{q},\omega)$ for silicon.
10. Perspective plot of $\epsilon_2(\vec{q},\omega)$ for a free electron gas.
11. Perspective plot of $\mathrm{Im}[\epsilon^{-1}(\vec{q},\omega)]$ for silicon.
12. Perspective plot of $\mathrm{Im}\left|\epsilon^{-1}(q,\omega)\right|$ for a free electron gas.
13. Plots of the zeros of $\epsilon_1(\vec{q},\omega)$ for silicon and a free electron gas in the (q,ω) plane.

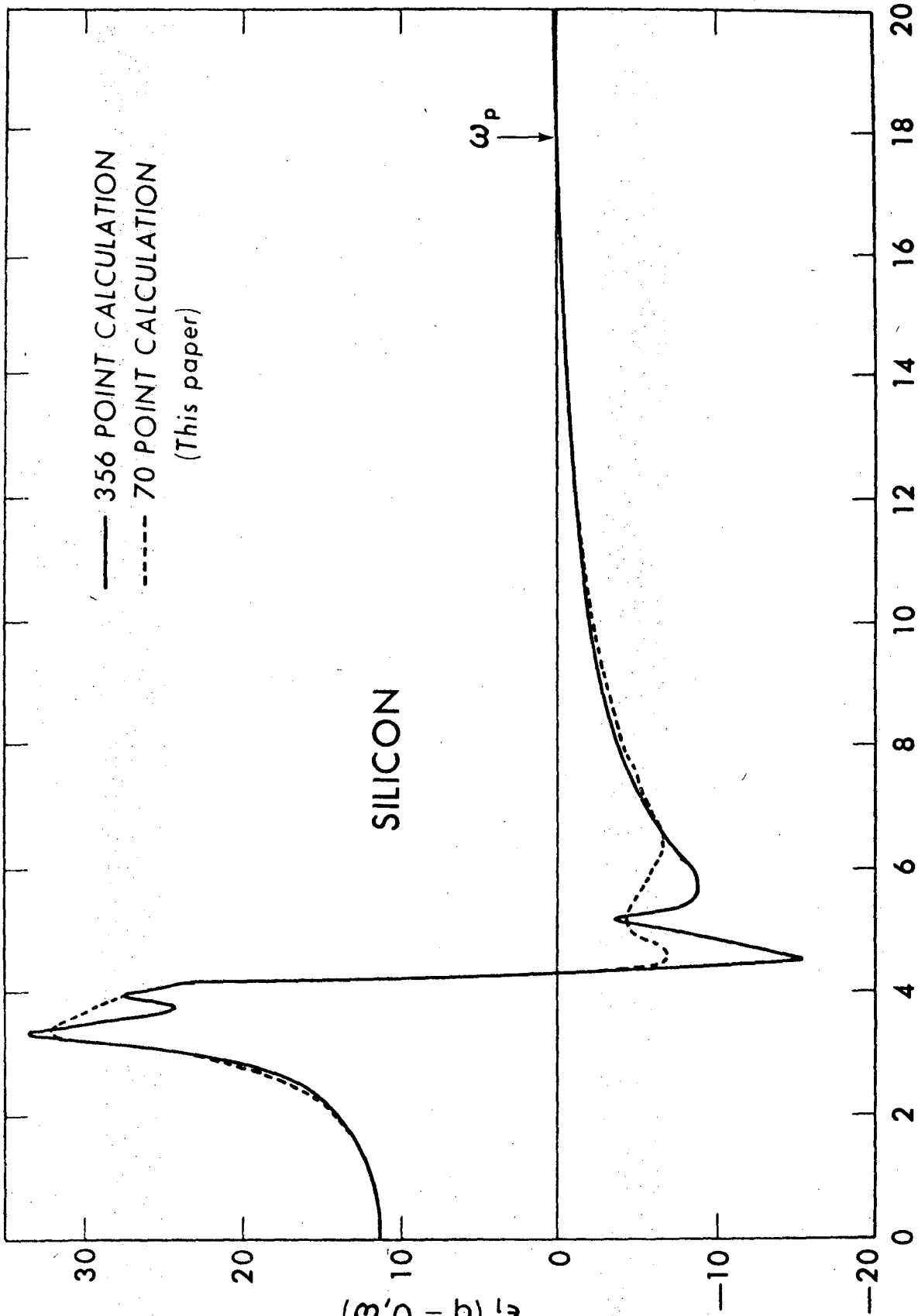
356 POINT CALCULATION
70 POINT CALCULATION
(This paper)
SILICON
ω_p
$\hbar\omega$ (eV)
ϵ_1 (q = 0, ω)
30
20
10
0
−10
−20
0
2
4
6
8
10
12
14
16
18
20

Fig. 1

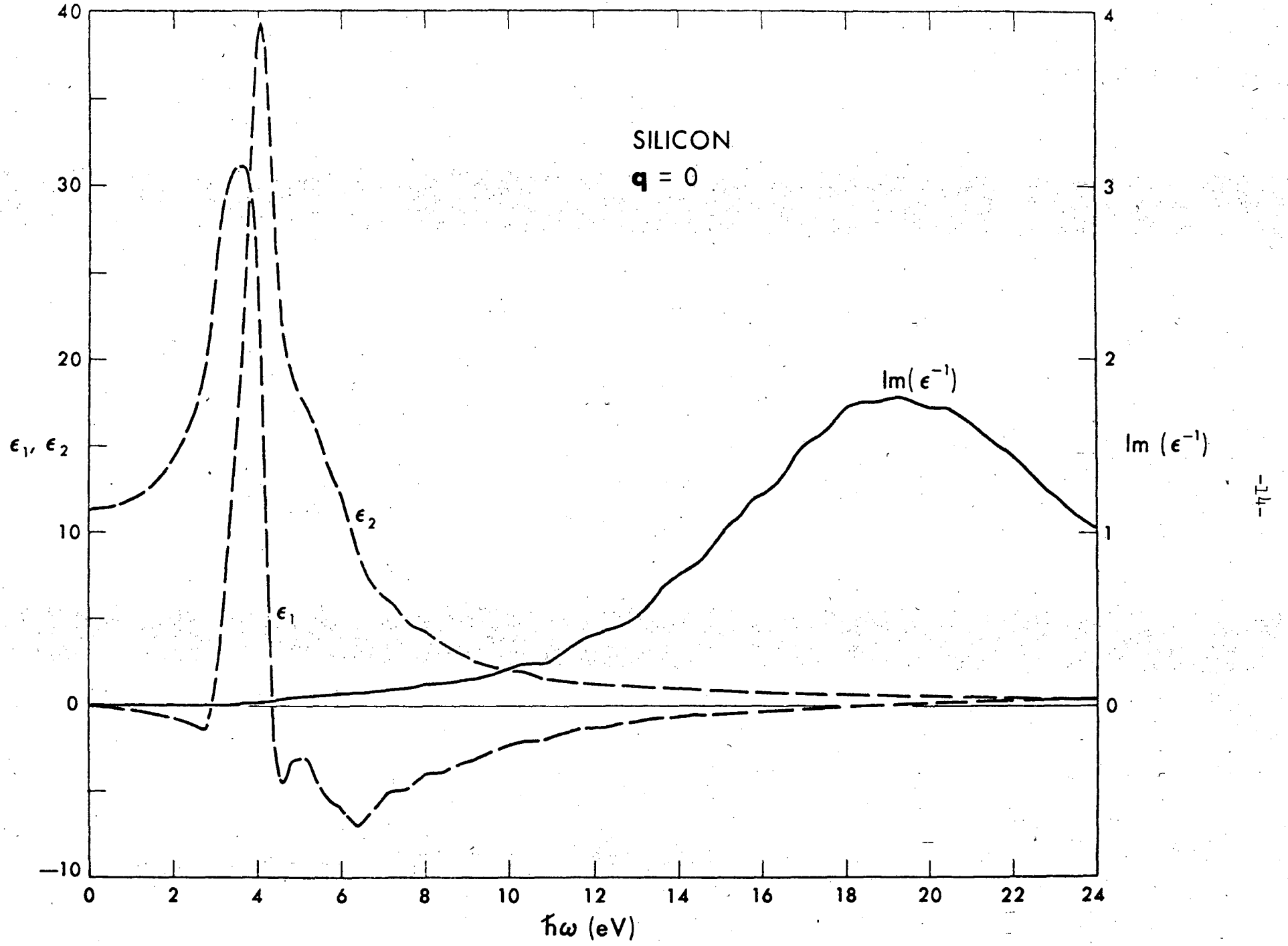
SILICON
q = 0
ϵ_1, ϵ_2
ϵ_2
ϵ_1
$\mathrm{Im}(\epsilon^{-1})$
$\mathrm{Im}\ (\epsilon^{-1})$
$\hbar\omega$ (eV)
40
30
20
10
0
−10
4
3
2
1
0
0
2
4
6
8
10
12
14
16
18
20
22
24

Fig. 2

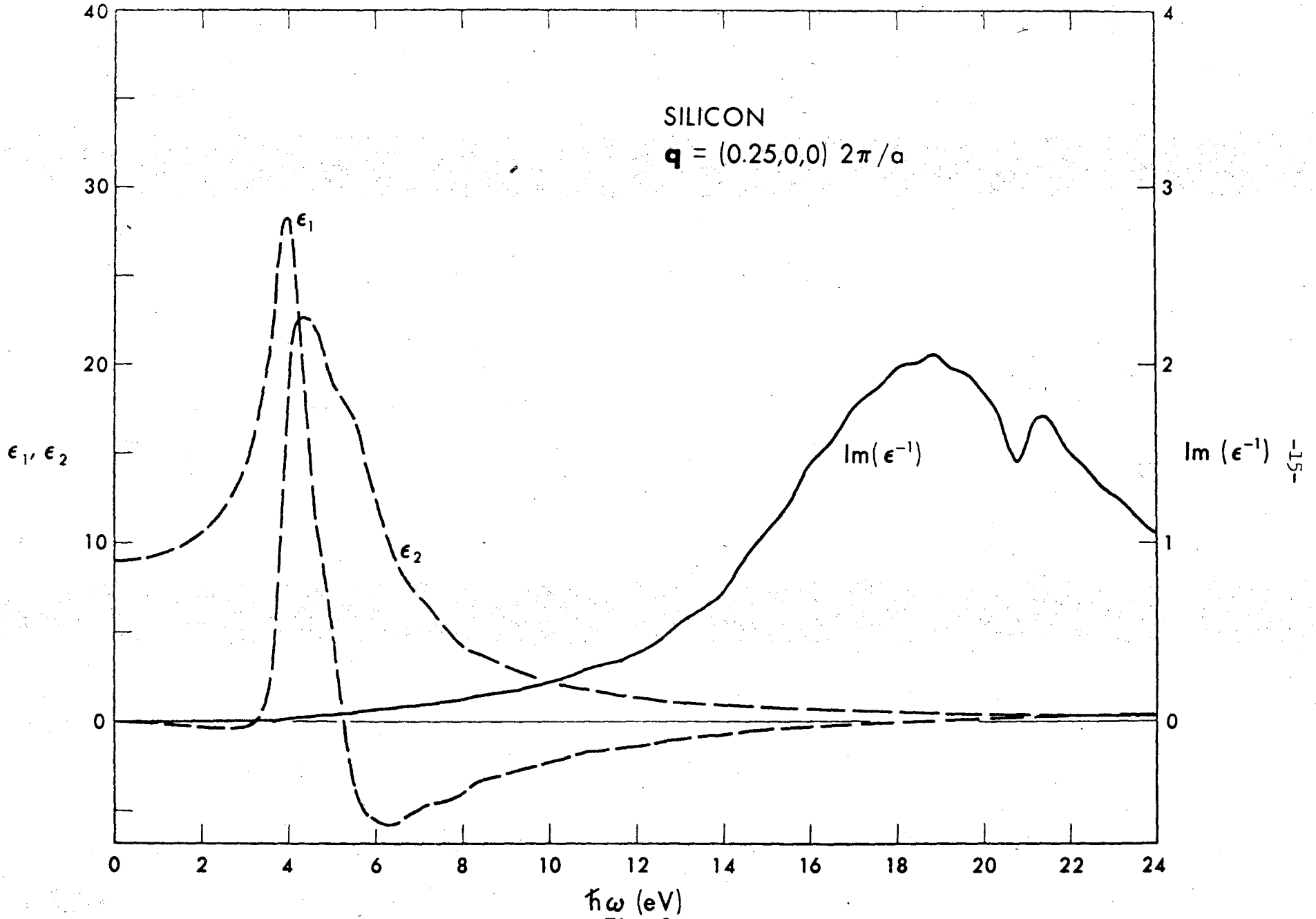
SILICON
q = (0.25,0,0) 2π/a
ε1
ε2
Im(ε⁻¹)
ε1, ε2
Im (ε⁻¹)
ħω (eV)
40
30
20
10
0
4
3
2
1
0
0 2 4 6 8 10 12 14 16 18 20 22 24

Fig. 3

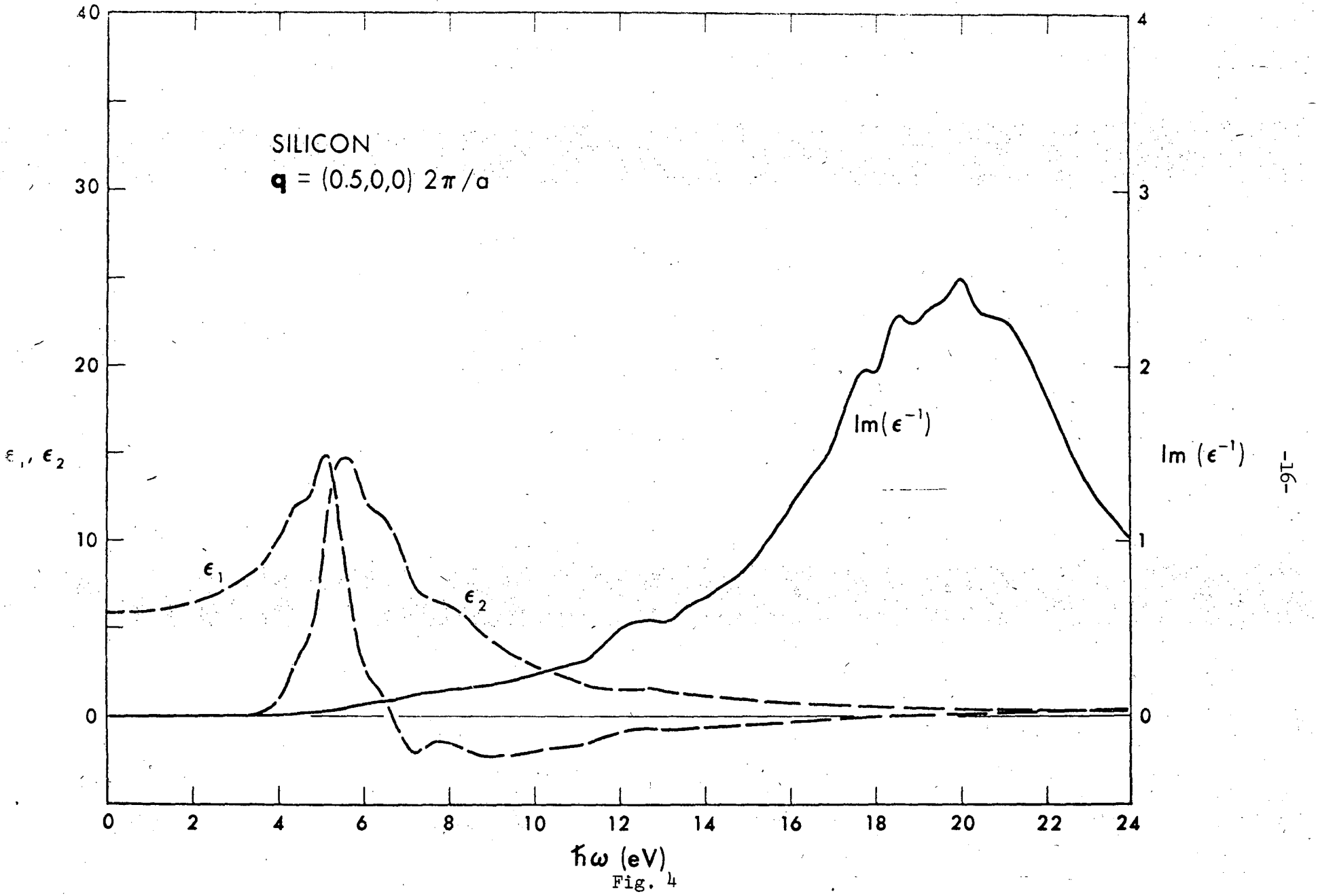
SILICON
q = (0.5,0,0) 2π/a
ε1, ε2
Im(ε⁻¹)
Im (ε⁻¹)
ε1
ε2
ħω (eV)
40
30
20
10
0
4
3
2
1
0
0
2
4
6
8
10
12
14
16
18
20
22
24

Fig. 4

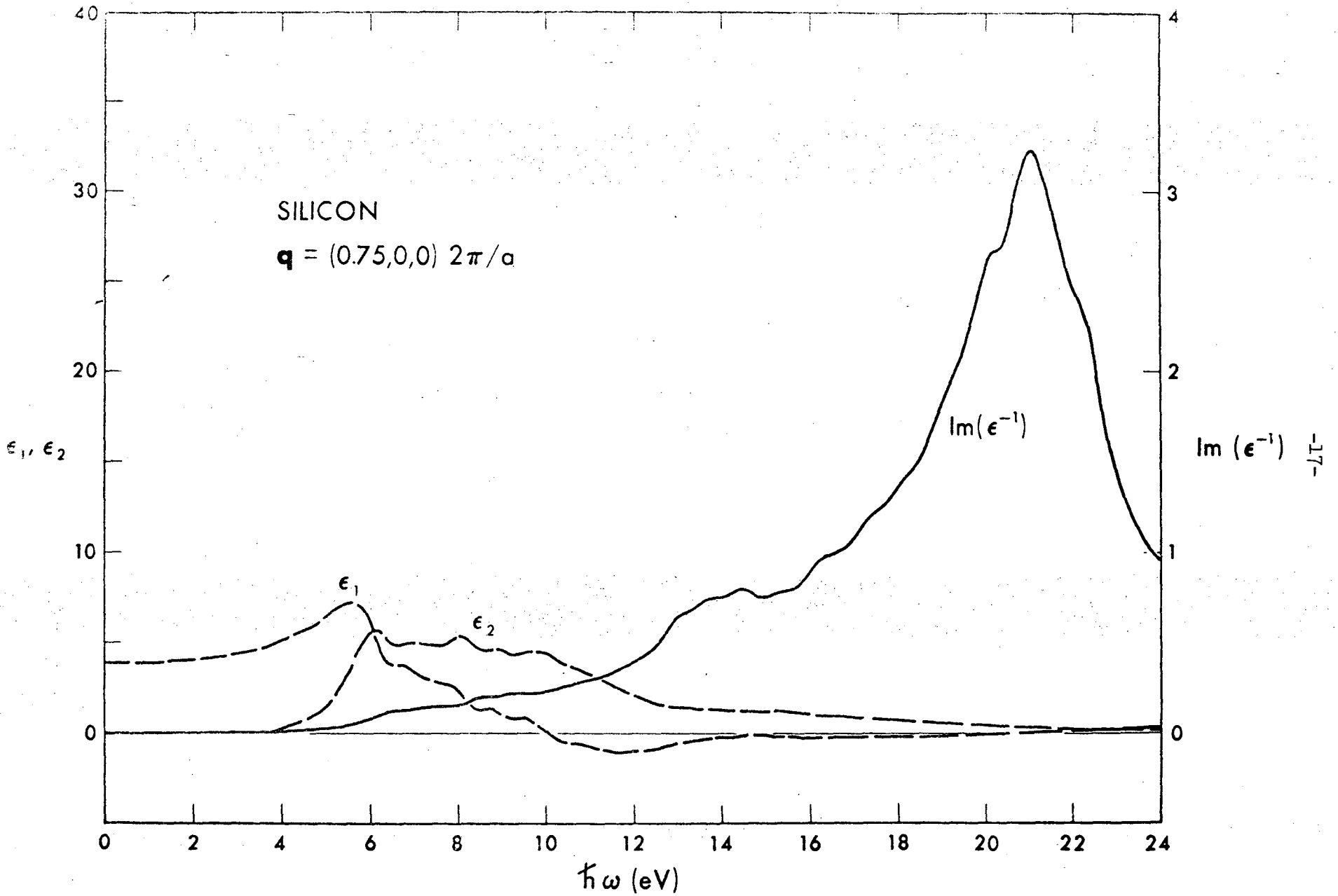
SILICON
q = (0.75,0,0) 2π/a
ε1, ε2
Im(ε⁻¹)
Im (ε⁻¹)
ħω (eV)
40
30
20
10
0
4
3
2
1
0
0 2 4 6 8 10 12 14 16 18 20 22 24

Fig. 5

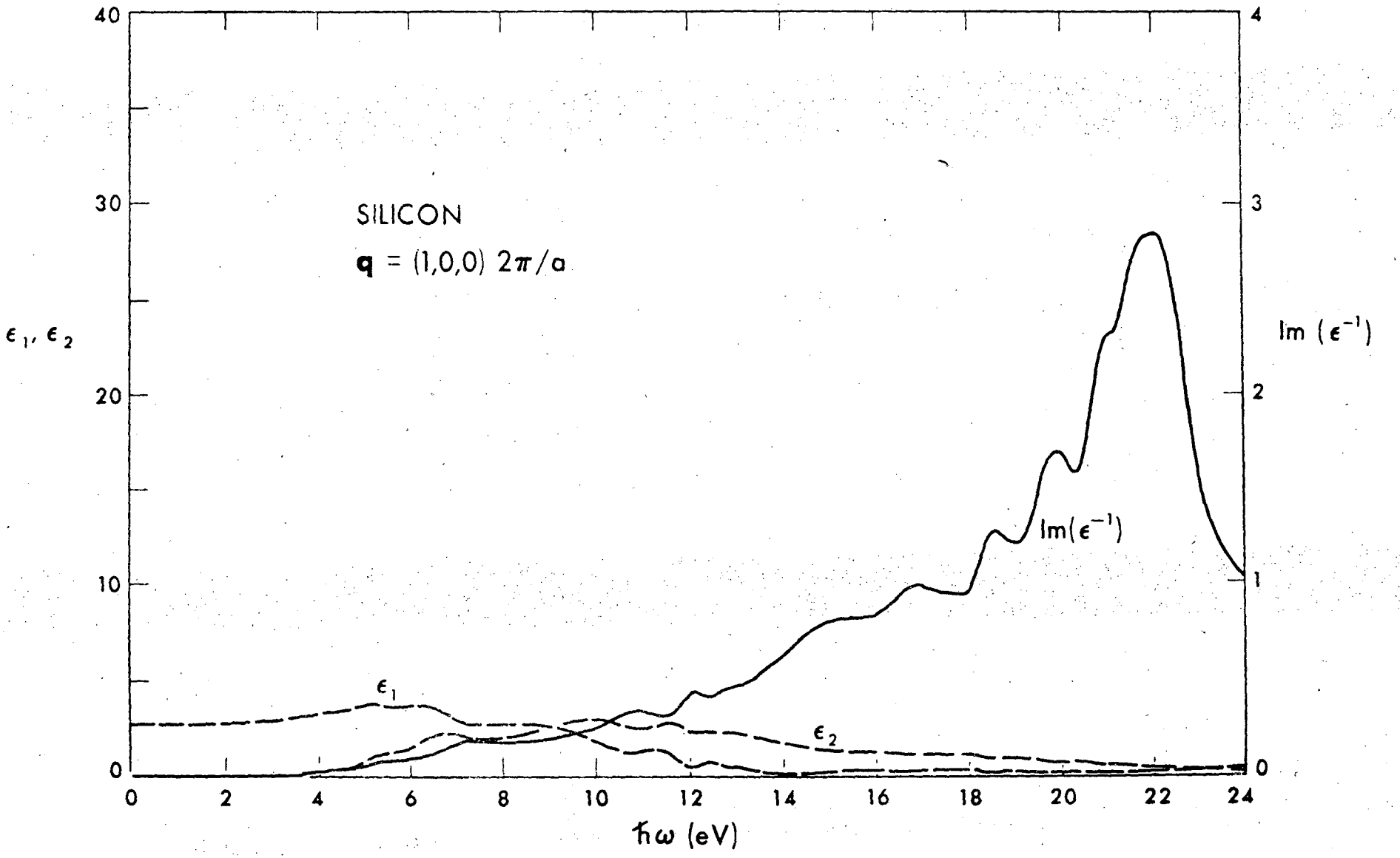
SILICON
q = (1,0,0) 2π/a
ε1, ε2
Im (ε⁻¹)
Im(ε⁻¹)
ε1
ε2
ħω (eV)
0
2
4
6
8
10
12
14
16
18
20
22
24
10
20
30
40
1
2
3
4

Fig. 6

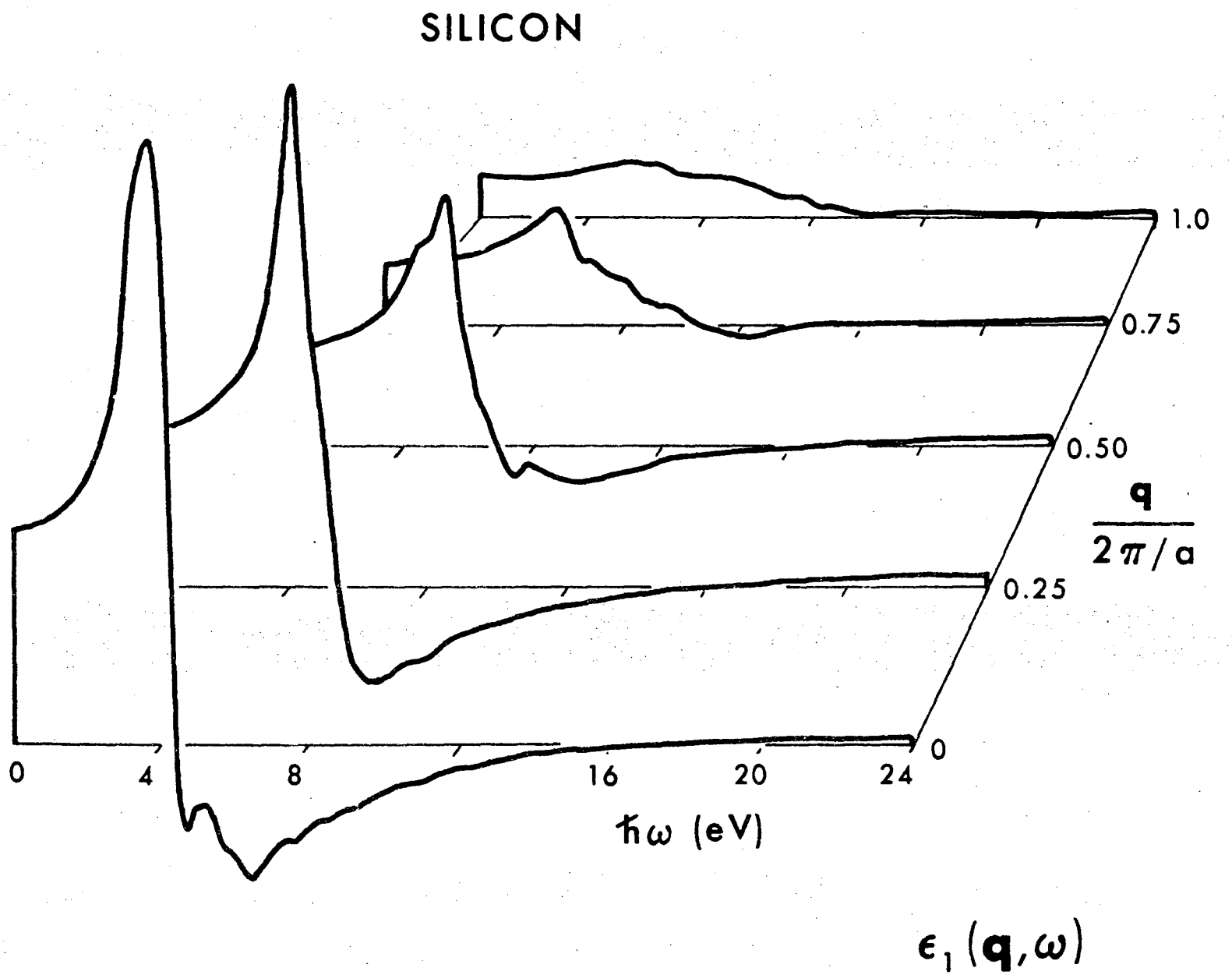

Fig. 7

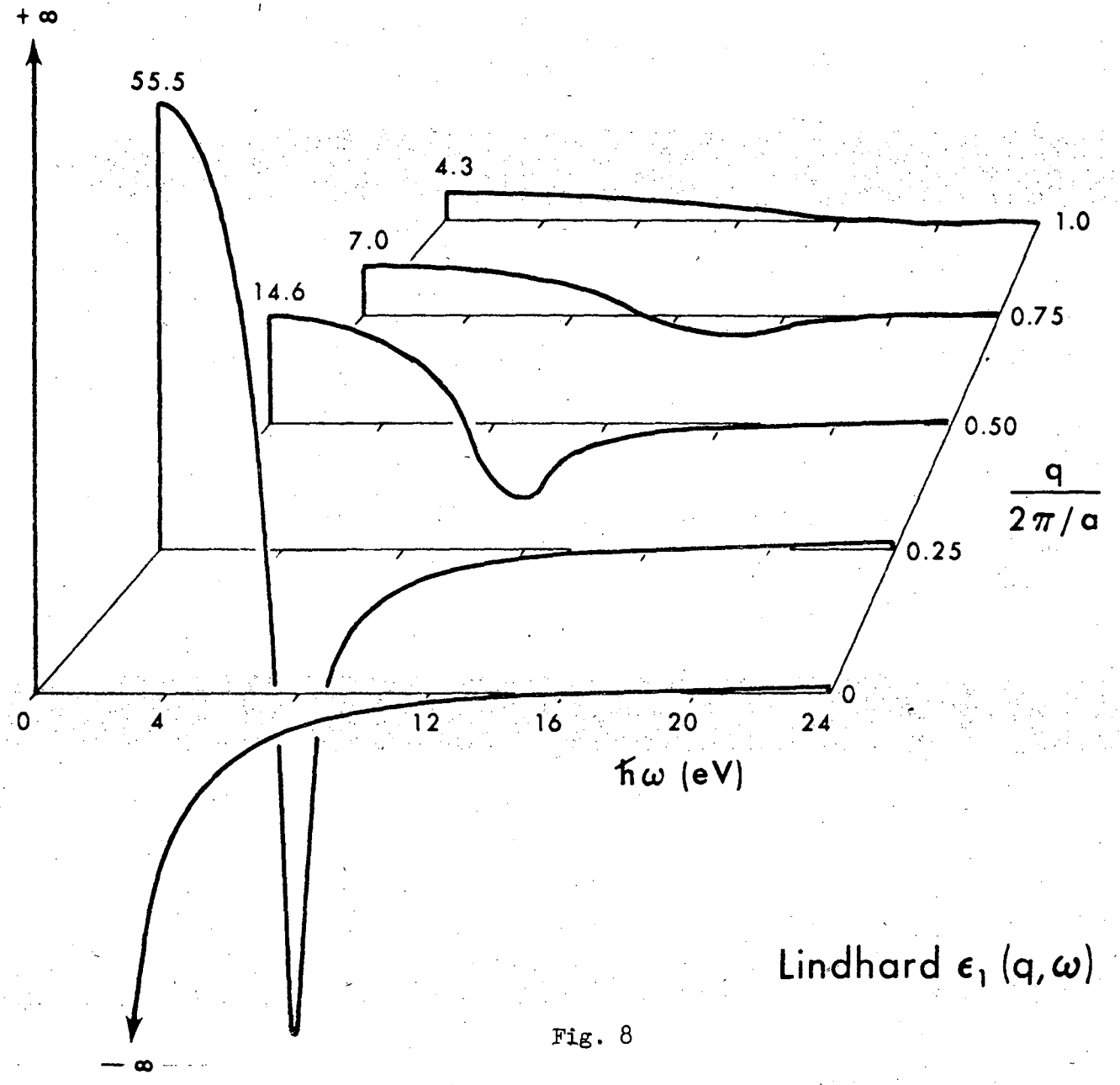
+ ∞
55.5
4.3
7.0
14.6
1.0
0.75
0.50
0.25
0
q / 2π/a
0
4
12
16
20
24
ħω (eV)
— ∞
Lindhard ε₁ (q, ω)

Fig. 8

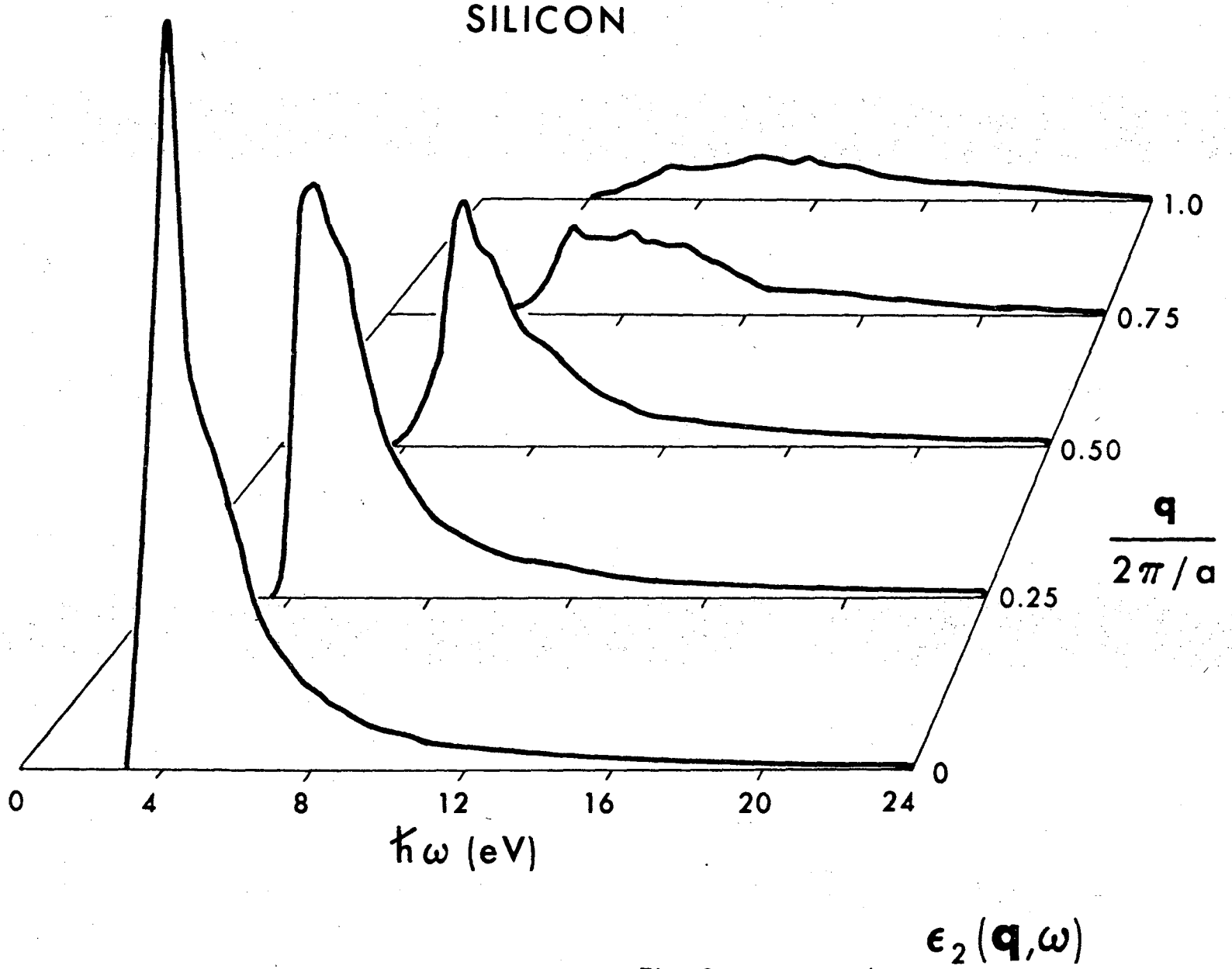

Fig. 9

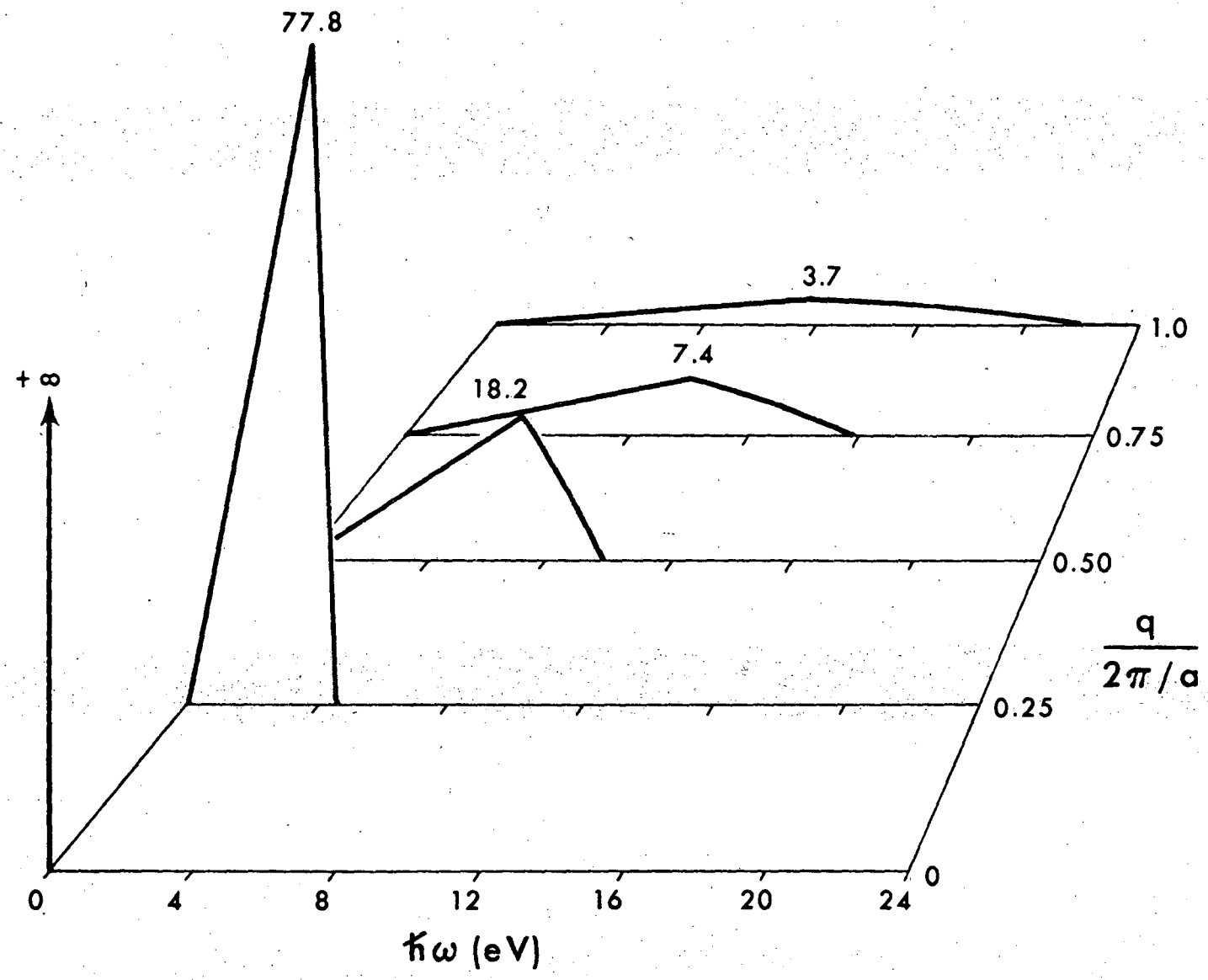

Lindhard $\epsilon_2(q,\omega)$

Fig. 10

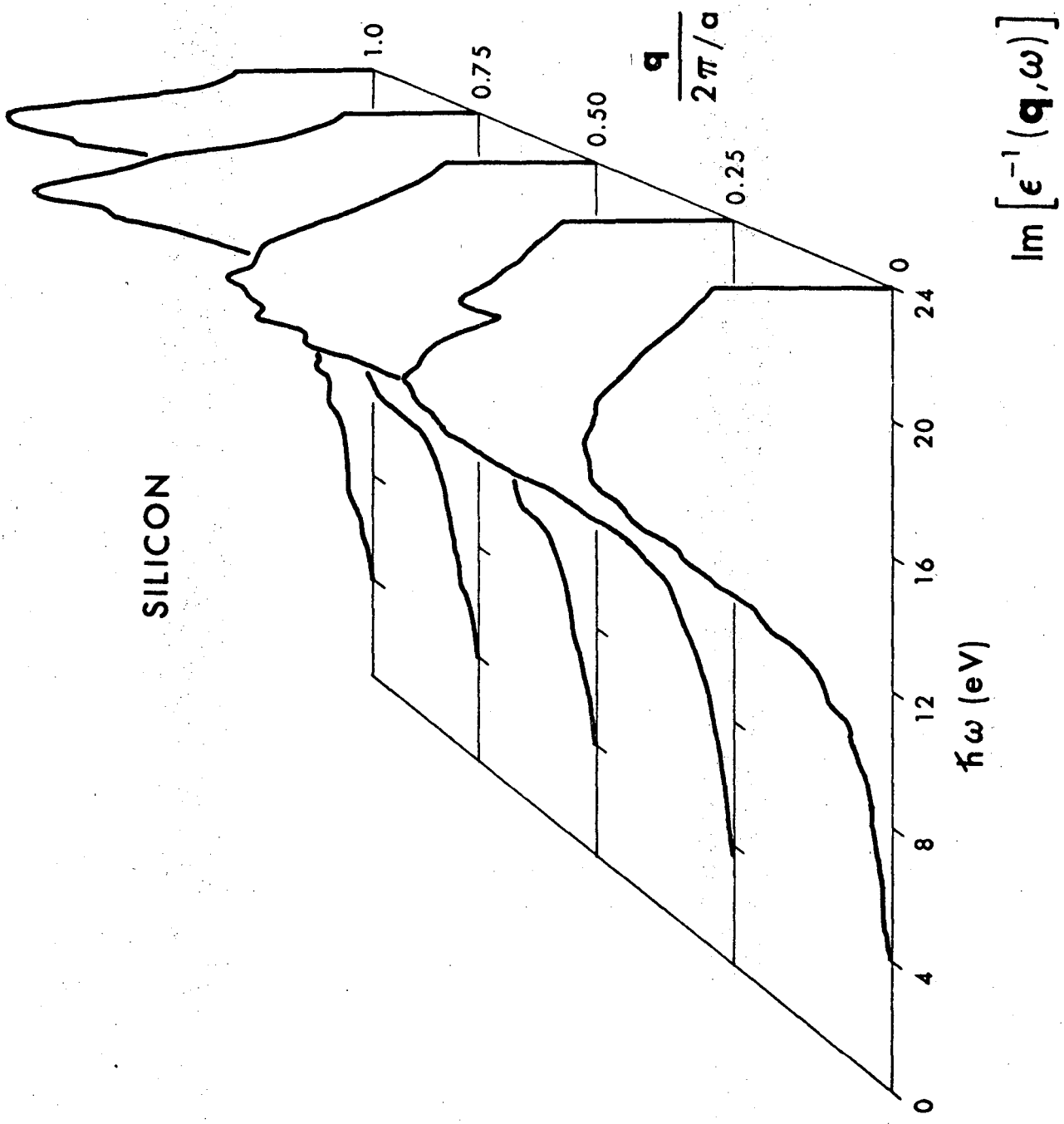
SILICON
1.0
0.75
0.50
0.25
0
$\frac{q}{2\pi/a}$
0
4
8
12
16
20
24
$\hbar\omega$ (eV)
$\mathrm{Im}\left[\epsilon^{-1}(q,\omega)\right]$

Fig. 11

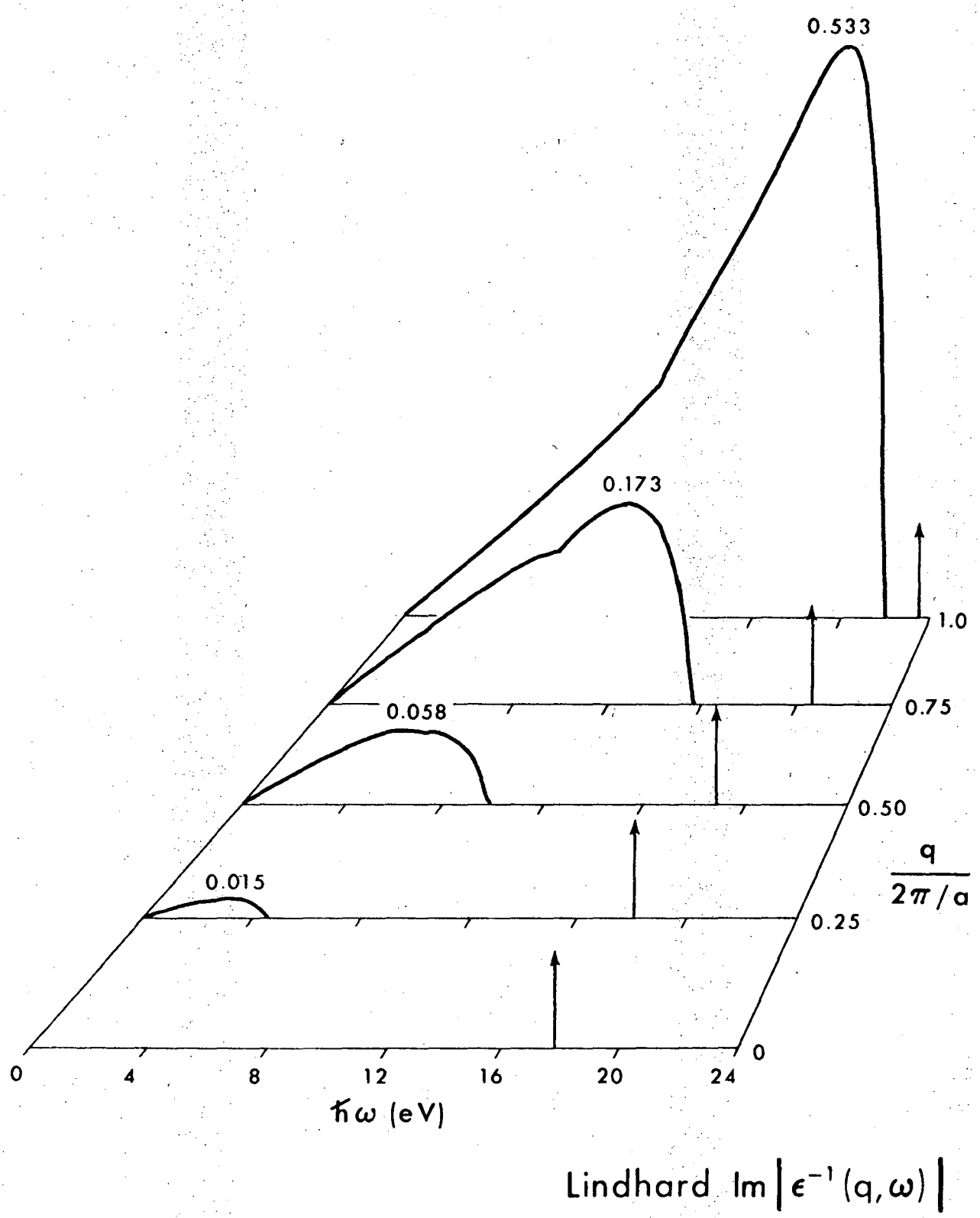
0.533
0.173
0.058
0.015
1.0
0.75
0.50
0.25
0
q / 2π/a
0
4
8
12
16
20
24
ħω (eV)
Lindhard Im|ε⁻¹(q,ω)|

Fig. 12

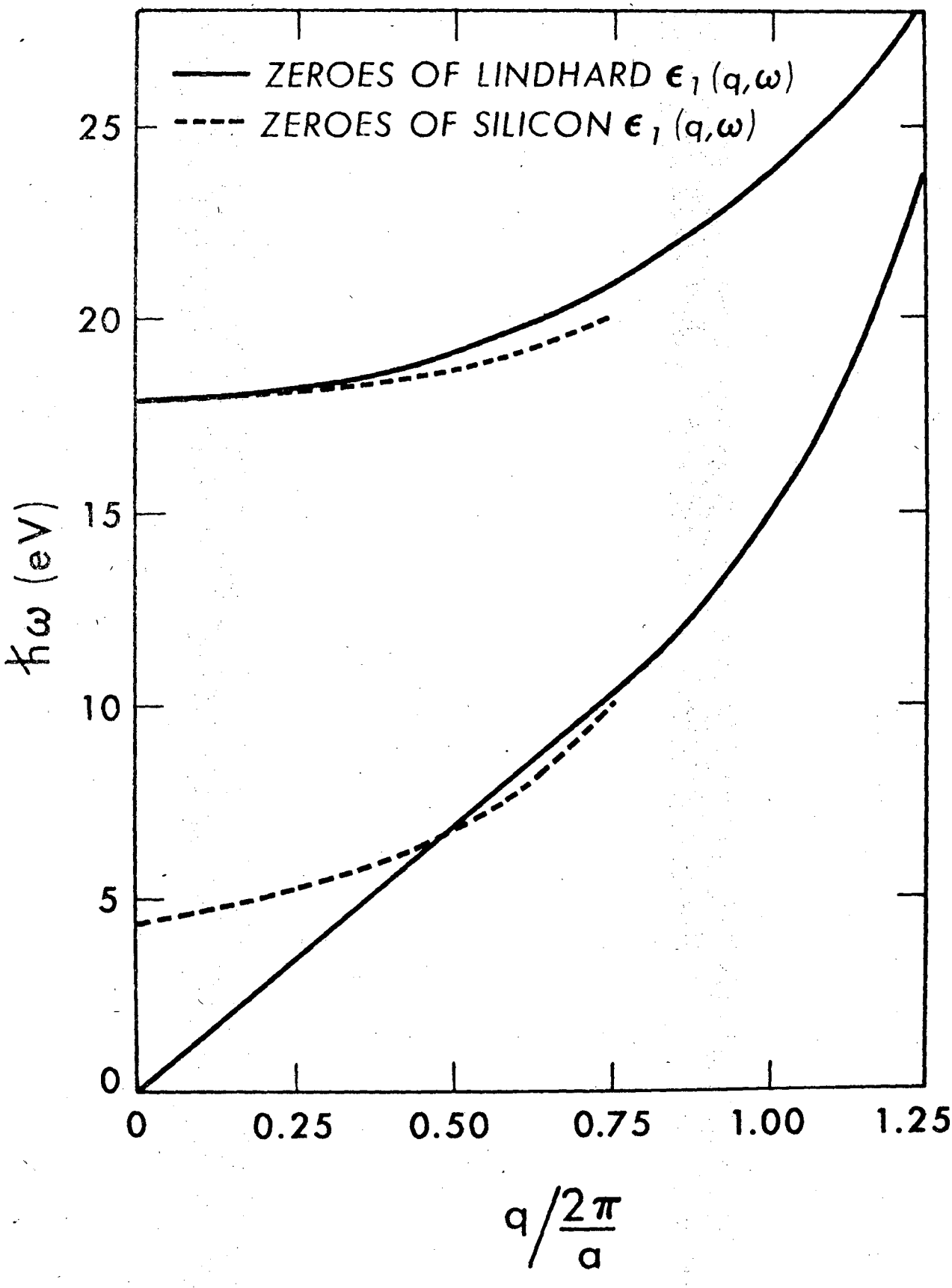
ZEROES OF LINDHARD $\epsilon_1(q,\omega)$
ZEROES OF SILICON $\epsilon_1(q,\omega)$
$\hbar\omega$ (eV)
0
5
10
15
20
25
0
0.25
0.50
0.75
1.00
1.25
$q/\frac{2\pi}{a}$

Fig. 13

LEGAL NOTICE

This report was prepared as an account of work sponsored by the United States Government. Neither the United States nor the United States Atomic Energy Commission, nor any of their employees, nor any of their contractors, subcontractors, or their employees, makes any warranty, express or implied, or assumes any legal liability or responsibility for the accuracy, completeness or usefulness of any information, apparatus, product or process disclosed, or represents that its use would not infringe privately owned rights.

TECHNICAL INFORMATION DIVISION
LAWRENCE BERKELEY LABORATORY
UNIVERSITY OF CALIFORNIA
BERKELEY, CALIFORNIA 94720